Image analysis system for acquiring three-dimensional contour of foot arch during balanced standing

Chi-Hsuan Lin[a], Jia-Jin Chen[a,*], Chi-Hsun Wu[a], Hsiao-Yu Lee[b],
Yuh-Hwan Liu[c]

[a] *Institute of Biomedical Engineering, National Cheng Kung University, Tainan, Taiwan, ROC*
[b] *Department of Management Information Science, Far East College, Tainan, Taiwan, ROC*
[c] *Department of Management Information Science, Chia-Nan University of Pharmacy and Science, Tainan, Taiwan, ROC*

Summary Compared to the X-ray approach, footprint analysis is a non-radiation and more viable method for clinical assessment of the medial longitudinal arch of the foot. In this study, we have designed an optical footprint acquisition system that consists of a digital camera and two pieces of glass, each with four load cells under each corner. When the subject stands on the transparent force plates, the digital camera is triggered, photographing the soles of the feet at the moment when both feet bear approximately at the same weight. A blue gel is placed between the foot and the force plate to enhance the contrast between sole and background. Based on the relationship between the brightness of the image and the thickness of the gel, the three-dimensional (3D) structure of the arch can be reconstructed which can provide more representative information than a conventional footprint image, with its low resolution and easy smearing.
© 2004 Elsevier Ireland Ltd. All rights reserved.

1. Introduction

The human foot exhibits a wider range of structural variation than almost any other part of the body. One of the most important and most variable structural characteristics of the foot is the height of the medial longitudinal arch (MLA) [1]. The foot arch provides the plantarflexors enough mechanical advantages to lift the weight of the body and absorbs the shock caused by upright striding during weight-bearing activities [2]. Increase in activity-related injuries has been associated with foot arch structures that are either too high or too low [3—5]. Additionally, mechanical modeling of the arch as a simple truss-and-beam structure indicates that lower strain energy storage in both low- and high-arched feet are prone to more injuries than a normally arched one [6,7]. Furthermore, inappropriate force produced by ground reaction force could impact calf muscles, knee joints and hip joints while walking. One of the common symptoms seen in the children during their development of bipedal walking is the flat foot. Children with flat feet usually develop an awkward gait, for example,

*Corresponding author. Tel.: +886-6-2757575x63423;
fax: +886-6-2343270.
E-mail address: jason@jason.bme.ncku.edu.tw (J.-J. Chen).

walking ''toeing out'' or lacking ''spring'' to push off, which can lead to frequent falls to the ground [8].

The most common approach for clinical diagnosis is to observe the structure or the appearance of the foot. However, subjective assessment through visual observation depends on the experience of the clinician. In addition to visual observation, various approaches have been developed to directly or indirectly measure foot abnormalities. Direct approaches, including anthropometric [9] and radiographic techniques, measure the longest distance of the arch and several defined angles from the two-dimensional sagittal section of the foot [9—14]. Compared to the anthropometric approach, measuring the indices from the outer anatomic landmarks of the foot, lateral X-rays provide a clear view of internal foot landmarks for obtaining the MLA structure information, e.g. Calcaneal angle, height-to-length ratio, and calcaneal-first metatarsal angle [9]. Currently, the radiographic approach is generally considered as the clinical gold standard for describing MLA because it provides consistent reliability and a strong correlation between radiographic parameters and injury of the lower extremities. Although the radiographic approach has good reliability while performed by an experienced technician, it has the disadvantages of being time-consuming, high cost, providing only the lateral view of the foot, and most importantly radiation exposure.

Compared to the lateral view of the foot taken by direct measurements, indirect approaches, including footprint [1,10,15—21] and photograph analysis [22,23], usually acquire two-dimensional (2D) information of the plantar surface of the foot, i.e. the sole, for further clinical assessment. Several useful indices, such as footprint angle, footprint index, and arch index, have been derived for clinical assessments. Research has shown that the parameters derived from footprint analysis correlate highly with those obtained from radiological techniques [10]. Compared to the direct radiological techniques, the footprint method is relatively simple, cost-effective, portable and is free of radiation. In addition, the footprint index also provides indirect information about abnormalities in arch height. These features make the footprint index the most commonly used assessment tool in daily clinical examinations of foot abnormalities. However, the conventional Harris and Beath footprint [24], or other alternative ways, to imprint the plantar surface onto paper have the same disadvantages: low resolution, contamination, and poor reproduction due to the body sway which occurs when standing on one leg during the sampling processes.

Researchers have pointed out that the footprint sampling process, when the subject is using freely chosen stance, might cause an inconsistent imprint. Inconsistencies in the measured footprints are likely to be influenced by the standing posture the individual habitually uses [1]. Hence, researchers have suggested taking the footprint while the subject is in a ''half body-weight stance'' by placing a portable scale under one foot. However, much care must be taken not to 'overshoot' with the transfer of weight. It is also commonly seen in clinical evaluations that an increase in body sway induced by one-leg standing during the sampling process may generate misleading data. These potential inconsistency problems during the imprinting process of a footprint might be part of reason for the controversy over the applicability of footprint analysis. In addition, clinical use of the footprint index is commonly determined by manually drawing the critical lines on the imprint paper, which is difficult to store for long-term progress monitoring of foot abnormalities.

Besides the 2D footprint, the human foot changes not only the imprint of its sole, but also its shape during growth. It is believed that three-dimensional (3D) information of the arch provides the most precise evaluation of changes in the foot. Despite its high cost and relative complexity, a laser scan can perform very well in 3D arch surface reconstruction. However, the laser scan can only be performed when there is not any medium between the scanner and the bare foot, i.e. without body support. A commonly demanded measurement in clinical usage is to evaluate the height of the medial longitudinal arch while standing with body-weight support, instead of in a posture that will give the true architecture of the arch. Although the 3D arch of the foot is an important factor for assessing the foot abnormalities, there is a lack of a convenient way to directly measure the contours of the arch of a standing human.

The aim of this study is to develop a footprint image acquisition system which can provide a footprint image with a higher resolution than the conventional ink mat while the subject is in standing balanced. From the 2D image of the plantar surface of the foot, the footprint index can be automatically measured to avoid the uncertain inter-examiner variation. Also using the same apparatus, a novel approach that utilizes a contrast medium to measure the depth of arch is validated in this study. Using a viable calibration processes, a 3D image of the arch can be reconstructed. Based on the 3D footprint contour image, new indices for measuring 3D arch volume can be developed for future clinical assessments.
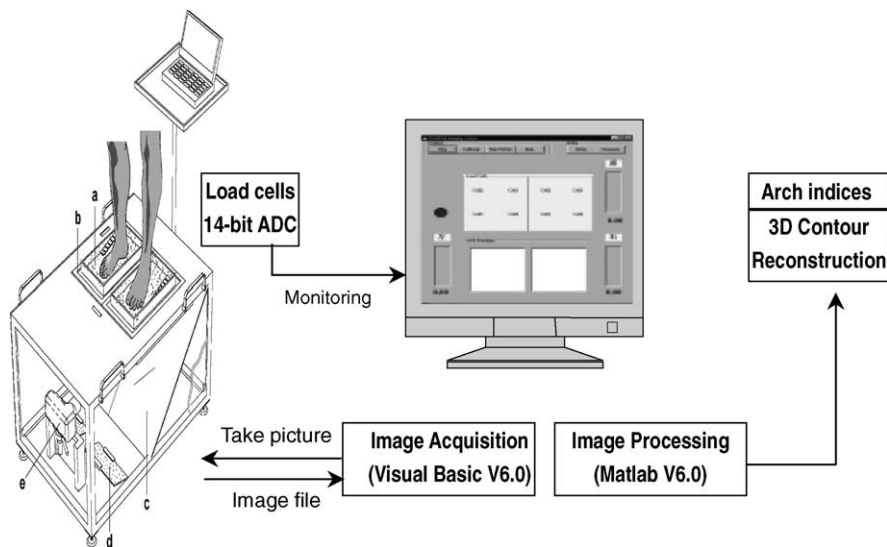
Fig. 1 Schematic diagram of footprint image acquisition and analysis system. The testing subject stands on the footprint image acquisition platform which consists of: (a) contrast medium, (b) force plates, (c) reflection mirror, (d) light source, and (e) digital camera. As soon as the subject is balanced, the digital camera will be automatically triggered to photograph the footprint image. The captured image is transmitted to a personal computer for further image processing using Matlab V6.0.

2. Materials and methods

2.1. Footprint image acquisition system

As depicted in Fig. 1, the footprint image acquisition system consists of four major components: contrast medium, force plates, light source with reflection mirror, and digital camera. A transparent box containing blue gel, called Putty, was placed between the foot and the force plate for better contrast. A light blue contrast medium can enhance the contrast of the sole's image in reflection to the surrounding contrast medium. The box of contrast medium was placed on top of two force plates encaged in a platform. The force plates, made of transparent glass with four one-axis load cells under each corner, were used to acquire the measurements of center of pressure and sway of the body. Each load cell (Transcell Technology Inc.) has a load capacity of 30 kg with rated output of 1.9998 mV/V. The analog outputs of load cells were sampled with a notebook computer via a 14 bit analog-to-digital converter. Because uniform distribution of light is essential for image analysis, we installed two tungsten lamps in front of the mirror, just next to the camera with frosted glass and several small surrounding mirrors. A mirror with $45°$ of tilting angle was placed under the force plate, in order to reflect the appearance of the soles of the feet to the digital camera (Kodak-DC4800) in front of the mirror. The camera has a high resolution of 2160×1440 pixels, corresponding to 0.3 mm resolution in the field of view (FOV) of $21\,cm \times 29.7\,cm$ (an A4 size paper). The camera can be triggered to take a picture by a software-developmental-kit (SDK) provided by the Kodak Company.

To acquire the footprint image, the subject statically stood on the transparent force plates with both feet in the contrast medium box within the arranged FOV while the weight loads on both force plates were monitored in real-time. As soon as the weight difference between the two force plates remained within 1 kg for three seconds, the digital camera was triggered to automatically take the footprint image using a program designed with Microsoft Visual Basic V6.0. The captured image was then transmitted to computer via USB interface for further image processing using Matlab V6.0.

2.2. Image processing for 2D arch indices

After acquiring the footprint image, the digital image processing was applied to detect the boundary of the foot and determine the critical points for deriving the arch indices. As mentioned above, the light blue Putty gel was put under the foot to enhance the contrast of the footprint image. For better performance and efficiency in separating the foot from the blue background, the captured image was first transformed from red—green—blue (RGB) to hue—saturation—value (HSV) space, which is very useful for working with color images to define visually interpretable object. The hue (H) characterizes the dominant color in which red is

assumed to be the reference. Therefore $H = 0$, 1/3, 2/3 correspond to pure red, green and blue color, respectively. The saturation (S) is a measure of the purity of the color. The S parameter depends on the number of wavelengths that contribute to the color perception. The wider the range of the wavelengths, the lower the purity of the color is. Similarly, the narrower the range of the wavelengths, the higher the purity is. The value (V) corresponds to the relative brightness in the sense of a gray value image. The extreme case $V = 0$ corresponds to the color black [25,26]. In our case, using the hue component was the most useful for separating foot (registered as orange) and the green distance-calibration markers from the blue background. Fig. 2(a) shows the histogram of the hue component of an *HSV* transformed footprint image. The color of foot, marker and contrast medium are arranged into the three primary colors, red, green and blue, from which the range of hue components between $0°$ and $360°$ is normalized to values between 0 and 1. Fig. 2(b) depicts the histogram of an original footprint image which can be clearly classified into three groups: foot sole ($H = 0 \sim 0.2$), the contrast medium ($H = 0.5 \sim 0.8$), the markers ($H = 0.3 \sim 0.5$). By a simple thresholding technique, four pairs of green markers each pair 2 cm apart can be separated and used to convert the units from pixel numbers to real length. Similarly, the sole of can be differentiated from the contrast medium for further extraction of footprint indices. A series of image processing techniques can be taken to determine the boundary of the foot sole for measuring the arch indices.

Several arch indices have been developed for the clinical assessment of foot abnormalities [1,10,16,17]. Among them, the foot angle and the arch index are both commonly used in clinical evaluations. The footprint angle, defined as the angle between the line connecting the most medial points of the heel and metatarsal region (a tangential line of the medial border) and the line connecting the most lateral point on the medial foot border to the most medial point of the metatarsal region. The arch index measured the width of the non-contact arch area at its widest part, as well as the width of the footprint at its narrowest part, to grade the footprint [10,16,17]. Typically, these indices were measured manually. For automatically measuring the arch indices, the primary process is to determine the tangential line of the medial border of the foot. As line AB shows in Fig. 2(c), it is drawn between the most medial points of the heel and metatarsal region. To acquire this tangential line we have adopted a mathematical morphology approach, the convex hull method. The convex hull is formally defined as a set of points having the smallest convex polygon set that includes the testing object, the footprint image in this case. The convex hull method scales the size of the hull with respect to the foot shape, and counts the number of intersections between the outline of the hull and the image. The convex hull approach can find a set of vertices that form the smallest convex polygon bounding the footprint by connecting all the vertices. Clearly, the tangential line is the one of the edges of the polygon that has the longest distance in the medial border of the footprint.


(a) (b) (c)
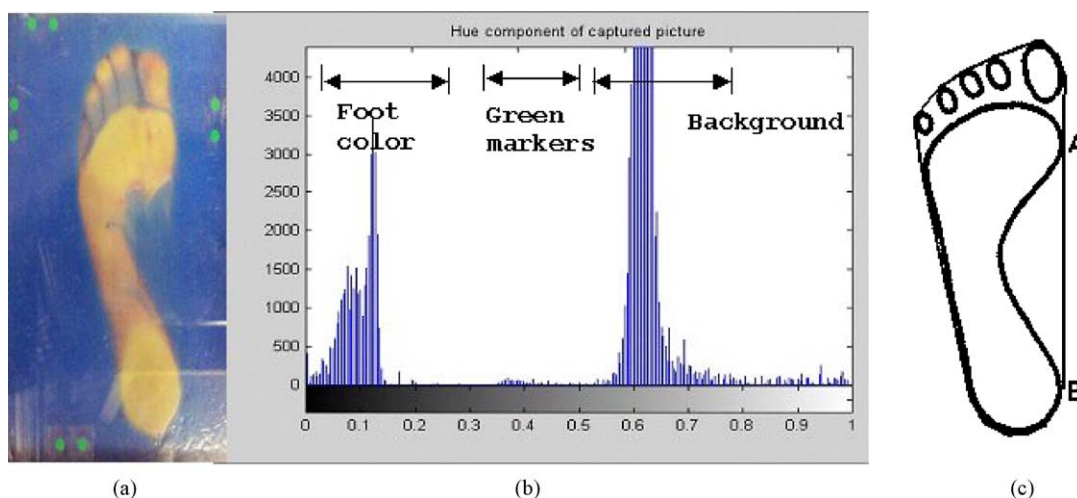
Fig. 2 A contrast medium is used to enhance the color image of footprint in (a). Three main clusters of hue component, i.e. the foot sole, green markers, and the contrast medium can each be clearly observed in the histogram of the hue component (b). Image processing techniques are used to determine the edge of the foot print for deriving the tangential line connecting the most medial points of the metatarsal (point A) and heel region (point B).

2.3. Image processing for 3D reconstruction of the plantar surface of the foot

A 3D reconstruction made from an object's surface image has been applied in various medical imaging fields [27−31]. These processes can be characterized by an analysis of the depth values or the distance to individual points on the object's surfaces. Some well-developed but complicated approaches use stereo images taken by two or more cameras and shape-from-shading technique for estimating 3D depth [32−34]. Using the same concepts, an alternative 3D reconstruction technique, which utilizes the relationship between depths and brightness, has been developed in this study. This is another key feature of using the Putty gel, in which the light intensity is presumably exponentially attenuated throughout this homogeneous medium. According to the relationship between depth and brightness, the height of the foot arch and its 3D surface contour could be reconstructed from the image of image. To establish the actual relationship between the depth of the blue gel and the brightness levels in the footprint image, a white descending stair, with thickness of 2 mm in the first five steps and 5 mm in the others, was designed, as shown in Fig. 3. This calibration step wedge was fixed in the blue gel up-side-down and was photographed simultaneously with the foot in order to minimize the picture taking variations between imaging sessions. First, the average brightness for each step was calculated; once the height and average brightness of each step is known, a cubic spline interpolation could be applied to relate the depth of the blue gel under each step to the average brightness in the image. Thus, using this derived calibration curve, reconstructing of the 3D image under the foot arch becomes feasible.

For evaluating the accuracy of the reconstructed 3D arch from the footprint image in our system, we utilized two acrylic arch phantoms, 2.5 and 1.2 cm in height to simulate the high and low arches of the foot. Using a laser scanner with a high resolution of 0.5 mm/dot, the arch phantoms were scanned as gold standards. To compare the models acquired from the laser scanner (laser-scan model) with those acquired from the footprint image (footprint model), coordinate transformations with three-axis rotations and translations were applied to transform the base of the laser models to the XY-plane. Cross-correlation was used to get the best corresponding position for surface matching, as well as for point-to-point error estimation. The volume enclosed by the surface of the arch phantom was also calculated. The discrepancies in volume under phantoms between the two measuring methods, i.e., the laser scan and our proposed 3D image reconstruction, were used as our performance measurement.
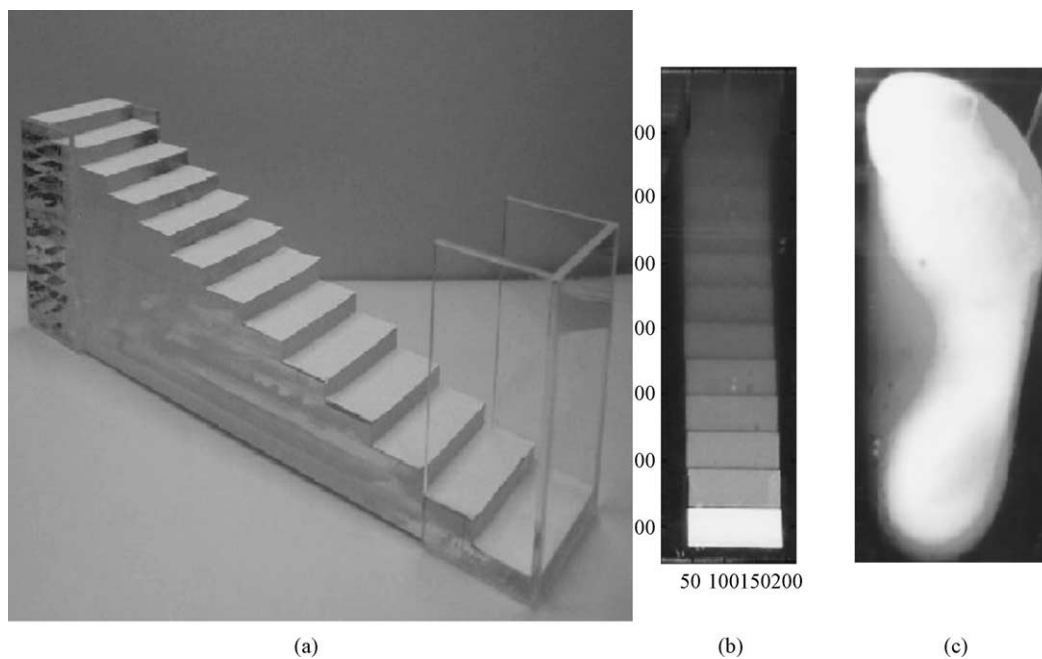
Fig. 3 (a) A descending stair is designed with varied levels: a height of 2 mm in the first five steps and 5 mm in the others for calibration purpose. (b) This calibration step wedge is placed up-side-down on the contrast medium and would be photographed simultaneously with the footprint image (c).

3. Results

3.1. Validation of footprint image acquisition setup

To minimize the distortion in the footprint's image, the control of ambient light and other picture taking conditions (e.g., the distance from camera to the object, exposure time, aperture, etc.) all need to be taken into account. For our light source, we must make the brightness of the light source as even as possible. The following procedures were used to verify the uniformity of the light source in our system. First, we put a homogeneously white A4 size of paper on the transparent force plate. Second, the digital camera was triggered to only take pictures with an exposure time of 1/180 s to avoid over-scaling of the brightness. Lastly, the entire image inside the selected FOV for covering the entire footprint image was divided into 10 × 10 grids. The mean value and standard deviation of the gray level of each grid were evaluated. The variance of the brightness is 14.5 with a mean brightness of 120.1. This results in a coefficient of variance around 12%. The variance within a grid is always less than two gray levels. This resolution is adequate to apply the thresholding technique to derive a footprint based on the histogram of the hue component of an *HSV* image.

3.2. Measurement of 2D arch indices

Fig. 4 depicts the detailed procedures for deriving the arch indices from the image of a typical foot sole, that is the original image after selecting the region of interest (ROI) and changing the pixel numbers to real length by using the green markers, as previously shown in Fig. 2. A simple threshold setting at an *HSV* value ranging between 0.5 and 0.8 can be easily used to transfer the hue
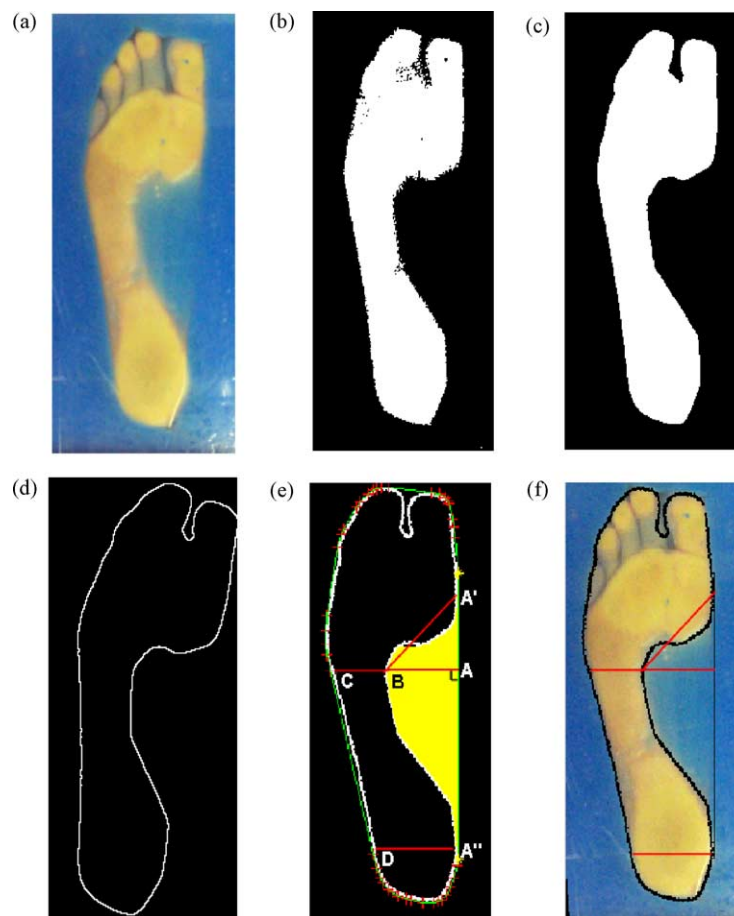
Fig. 4 Procedures for footprint image processing to derive the arch indices. The original footprint image (a) is transformed to a binary image (b) through a thresholding technique. The boundary of foot sole can be extracted after (c) median filtering and (d) edge detection processes. The convex hull method is applied to acquire the tangential line of the arch and then to derive several useful arch indices (e). The extracted boundary and indices match very well with the original image, as shown in (f).

component of the footprint's image (Fig. 4(a)) into binary format, as shown in Fig. 4(b). After eliminating noise by using a 5×5 median filtering, the initial boundary of the foot can be extracted. The boundary, after eroding the binary image with a 3×3 matrix structure element from detecting the boundary from the original one (Fig. 4(c) and (d)), is used for determining the footprint instep index and the area beneath the arch.

After determining the footprint boundary, a special problem for measuring the footprint index is determining the tangent line of the footprint arch. Our approach utilized an efficient convex hull method that finds a convex polygon by bounding the shape of the foot with the intersections (vertices) marked with crosses in Fig. 4(e). By connecting all the vertices, the outline of foot sole was surrounded by a polygon which had the smallest convex region of the boundary of the foot. The footprint's tangential line was defined as the longest line between two neighboring vertices. One of the vertices is at the most medial part of the fore of the foot (A′ in Fig. 4(e)) and the other is at the rear (A″). The most lateral point (B) of the concave region in the medial border of the middle part of the footprint can be found. The segment (AB) can be determined from point B in perpendicular to the tangential line (A′A″) with intersections at points A and C. Point D is then defined as a point, at which the line starting from point A″ and perpendicular to the tangential line interest the lateral border of the hind foot of the footprint. In this case, we obtain AB = 5.1 cm and BC = 3.4 cm

to be used as the arch index of Rose et al. [17]. Similarly, the arch index of Staheli et al. [16] is determined using the ratio of the line segment BC divided by A″D (5.5 cm) and is equal to 0.618.

In addition to the footprint index, several flatfoot assessment indices can also be derived. The footprint angle, as defined in [1], can be determined from the right-angled triangle (formed by points A′, A and B) as (AB/A′B) and is equal to 43.2° in this case. The above values are within normal range according to the research of Shiang et al. [35]. The arch area can also be acquired from the area surrounded by points A′, B, and A″, within which there are 5801 pixels, approximately an area of 4000 mm^2 in this case. The ratio of non-contact area (area encompassed by A′BA″) to contact area (the entire convex hull area) can be also calculated. Fig. 4(f) maps the footprint contour and the derived indices to the original footprint image, which ensures the correctness of the computation and overcomes the potential errors of manual operation.

3.3. Measuring the 3D contour of the plantar surface of the foot

Since the ambient light and picturing conditions might vary each time, the footprint images were always taken simultaneously with the calibration step wedge in each individual image, which alleviates the variations in picture taking conditions. The mean and standard deviation of the selected area of each calibration step, in a window size of 20×20

(a)   (b)
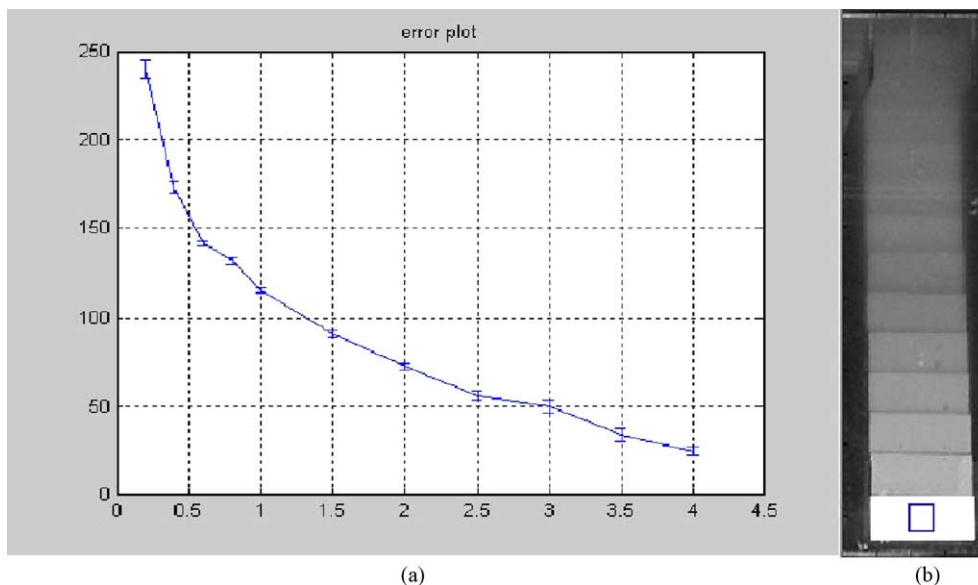
Fig. 5   The brightness-to-depth relationship of calibration step wedge is used for transforming the gray level to a depth measurement of the foot arch. The cubic spline approach is utilized to fit the measured gray levels, with error bars indicating the standard deviation in (a) which were obtained from the selected images of 20×20 window size from each stair of calibration step wedge in (b).

pixels, was calculated for the spline interpolation. As expected, the gray levels of each step of the calibration step wedge were distributed in an approximately exponential curve, as depicted in Fig. 5. The gray level values are distributed from 20 to 240 for the 0.2−4 cm calibration stairs. This range almost covers the entire range of gray levels that are needed for the 3D contour estimation. The cubic spline interpolation technique used in this study can approximate very well for the depth measurements. Using this calibration curve, we can reconstruct the 3D arch contour. Validation measurements were performed using the high and low-arch phantoms.

As shown in Fig. 6(a), the high-arch model obtained by laser scanner with 0.5 mm resolution is used as the standard model for error comparison. Fig. 6(b) shows the reconstructed model obtained by our footprint image acquisition system. The sur-

face of the laser model seems to be smoother than that of the footprint image. The 3D surfaces of the laser-scan and footprint models were aligned according to maximal cross-correlation value. The point-to-point discrepancies between the two models were measured for analysis. As shown in Fig. 6(c), surface matching for the laser model and the footprint model were projected to the YZ-plane. The mean errors for varied slices were from 0 to 2.6 mm (10% in height), as depicted in Fig. 6(d). Statistically, the mean error for 3D model was less than 1.03 mm (S.D. = 0.78), and the percentage of volume difference is 0.14. The overall volume of the footprint image model is 70.2 cm^3, which is extremely close to that measured in the laser model, 70.1 cm^3. Similar measures were carried out for the low-arch phantom. The observed comparison of the laser model and the footprint

(a)

(b)

(c)

(d)
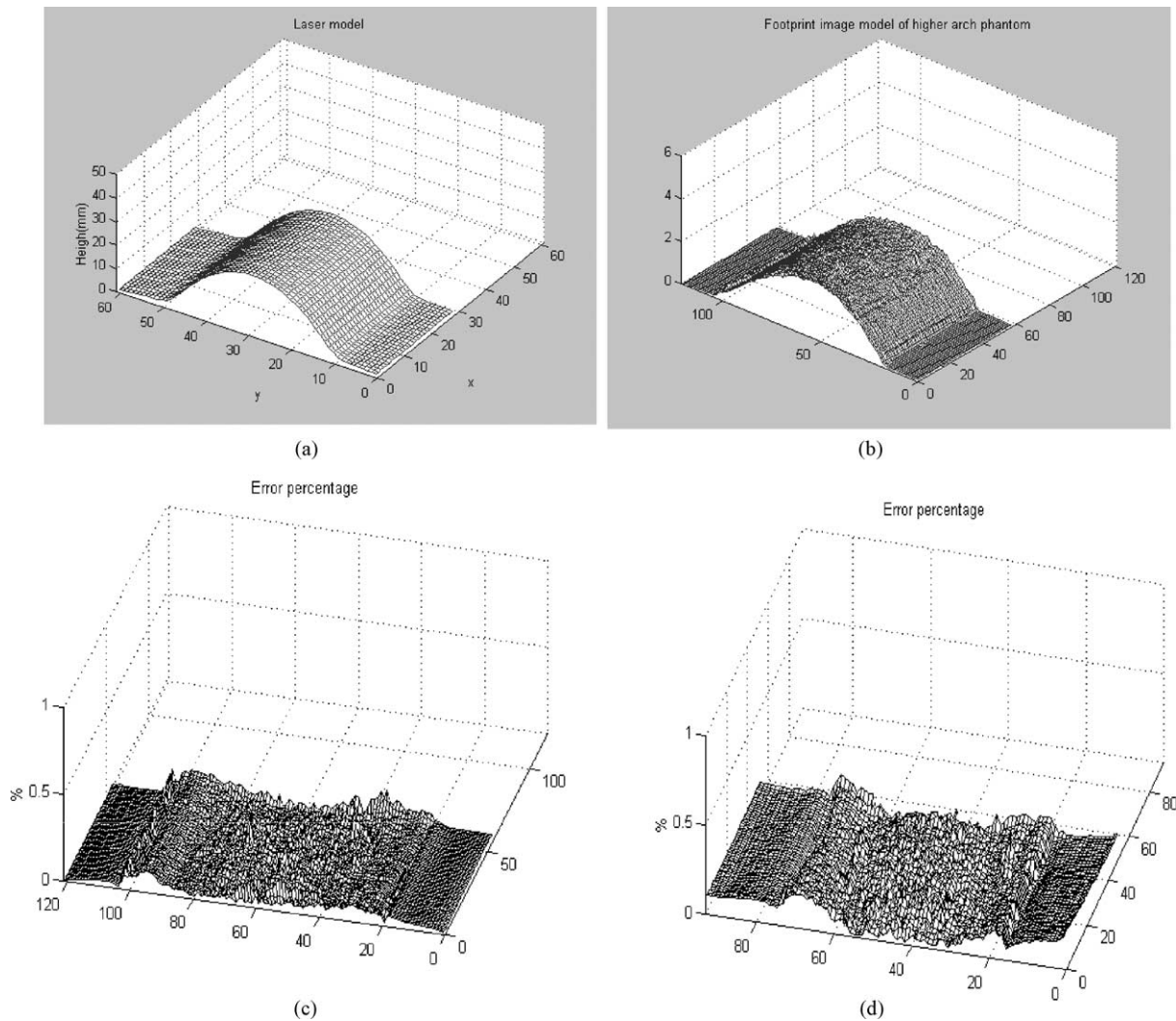
Fig. 6   The laser scan of a high-arch phantom (a) is used as a standard for validating the 3D contour derived from the footprint image (b). Disparities between the laser scan and the footprint image approaches for both (c) the high-arch model and (d) the low-arch model are less than 1%.
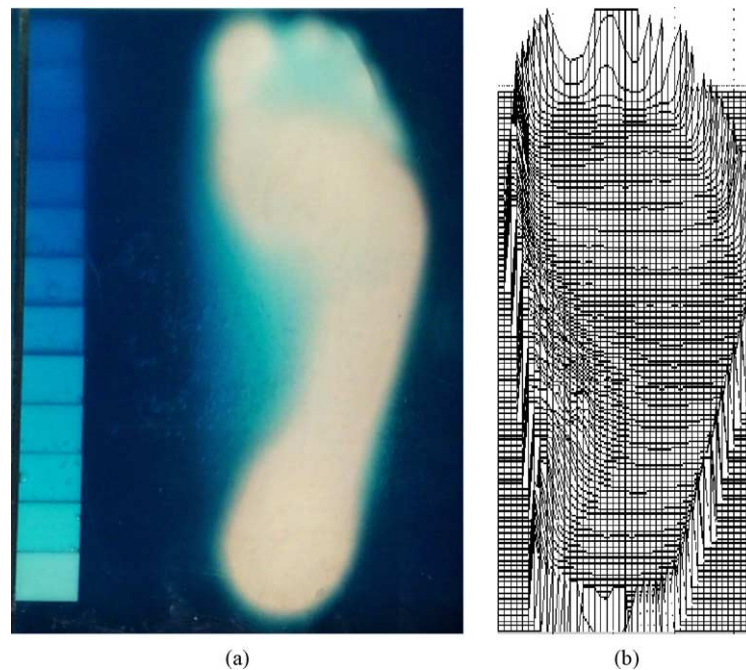
(a)   (b)

Fig. 7 The original of a weight-bearing footprint image (a) and its corresponding 3D contour reconstruction (b).

image model showed the mean errors for varied slices fell between 0 and 1.8 mm (15%), and the mean error for the overall 3D model was less than 0.8 mm (S.D. = 0.45). To check the validity of the reconstructed volume, the measured volumes were 22.1 cm^3 in the footprint image model, and 23.9 cm^3 in the laser model. The percentage error of volume difference was 7.5% in the low-arch phantom.

Using uniform diffused light and using a well-packaged box with high elastic rubber and homogeneous contrast medium, a weight-bearing surface model of a real foot was taken. Fig. 7 shows the footprint image and its constructed 3D contour, acquired by corresponding the image intensities measured at the arch region to relation curve. From the resulting image, it seems feasible to derive the 3D contour from a 2D image, but this needs more clinical trials for further evaluation.

4. Discussion and conclusion

The height of the medial longitudinal arch of the foot is one of the primary criteria for the diagnosis and classification of foot pathology. The traditional approach for footprint analysis, by taking an ink print of foot sole, is an inexpensive and easy way for a clinical approach. At present, however, there is some controversy in considering the validity and efficacy of using these standard footprint indices to predict arch height. Several researchers [1,15,16] reported that high correlation could be found between footprint parameters and arch height. However, others [18] reported very low correlation between navicular arch height and several footprint parameters. According to their studies, they opposed to the idea of using these indices for predicting arch height which. These conflicting interpretations might result from inaccurate footprint collection procedures and subjective drawings of the landmarkers. These footprint collection procedures inevitably produce low resolution, unreliable, and smeared footprint images because of the usage of ink and potential body imbalance during the taking of footprints. Furthermore, automatic detection schemes and 3D reconstructions used in characterizing the structure of the arch still lack sufficient clinical study.

In this study, a real-time footprint image acquisition system has been developed to overcome the disadvantages of the conventional footprint imprinting methods, and can derive the common footprint indices automatically. In our system, the picture of the sole of both feet is taken when body weight is equally borne on each foot to ameliorate the inaccuracies that result from this imbalance. In addition, the image is high resolution and non-contaminated. Considering the hardware, a mirror placed at a 45° angle ensures the least distortion from uneven reflection. Since the light control is very important, we performed our tests in a dark room. This can be improved by sealing the platform with black cloth. Additionally, using blue gel to enhance the contrast is a novel approach for

acquiring a footprint image with sharper contrasts which can facilitate the accuracy in further image processing.

Two critical approaches make our proposed image processing a successful approach in deriving 1D and 2D arch indices. First, the contrasts among 'green' markers, 'blue' gel, and the 'red' foot make the three subjects readily distinguishable according to the hue component of an *HSV* image. Next, the convex hull method is an effective approach to acquire the medial tangent line, which significantly reduces the errors resulting from manual drawing. In our system, three footprint indices were obtained automatically in accordance with those reported by other studies [1,16,17]. The ratio of the non-contact area to contact area is also derived, which is similar to the arch index of previous studies [17,35]. The only difference is that the contact area used in our system includes the toes because we were unable to separate them from the metatarsal region. Even though, it seems reasonable to use this index but it will require further clinical studies to define the normal ranges.

Based on the established relationship between the depth of the blue contrast gel and the brightness of the corresponding area in the image, 3D reconstruction becomes feasible. Although the laser scanner can reconstruct the surface of the bare foot better, it could not perform under weight-bearing conditions because the errors will increase greatly if a laser is projected through glass. In our system, the photograph represents the appearance of the plantar surface of the foot under normal weight-bearing conditions. For validation, we designed two arch phantoms with different heights that are rigid and will not change their shapes or sizes. The maximal mean errors of slices occur at both the turning points and the highest point. The former might be due to the smooth surface and reflective characteristics of the acrylic phantoms, which might affect the measured brightness. The latter, however, could result from insufficient gray level gradients in the blue contrast gel in the image at a higher depth level. This may be overcome by sharpening the slope of relationship curve by increasing both the light intensity and the concentration of the gel. In clinical observations, Shiang et al. [35] compared the correlations between arch height and eight commonly used footprint parameters and concluded that the correlation coefficient between arch height and any footprint parameters increased when more information was used to calculate the footprint parameters. These observations might imply that more dimensional data, such as 3D arch parameters, are essential for accurately estimating arch heights. Compared to our direct measurement of 3D arch height, foot pressure was generally used to estimate the indirect 3D information about the 3D arch.

Using our current measurement facilities, several clinical assessment features, including balance sway data as well as foot pressure, can be acquired simultaneously with the footprint image. It is well known that visual, somatosensory and vestibular systems are three important sensory sources, providing information about the body's spatial position and orientation in its environment. The abnormality in the foot arch will affect balance functions due to inappropriate somatosensory input. Children with flat feet usually suffer from an awkward gait, which might result in poor balance and cause them to fall easily. Since eight load cells have been installed under each corner of the transparent glass, it is feasible to monitor in real-time the center of pressure (COP) while static standing. Then, the sway path and area of the COP can be acquired in our flat foot image assessment system, which can provide essential information for correlating the 2D and 3D footprint indices with the balance evaluation in a single test trial.

In summary, a low-cost, fast and easily-operated image acquisition system has been developed which not only provides 1D and 2D footprint indices, but also estimates a 3D arch volume. These indices might be essential for the clinical screening of the pathology of the foot arch, and for deciding treatment protocol, as well as for follow-up studies. We expect that the arch volume might be more suitable for representing the foot arch function or abnormalities than standard 1D or 2D footprint parameters. This is because the volume beneath the arch is generally associated with the shape of the foot and hypothetically indicates shock absorbing ability. Furthermore, the 3D reconstruction model under weight-bearing condition can be used for computer-assisted design, fabrication, and manufacture of effective well-fitting insole pads or orthosis. Our ongoing project is to combine the balance assessment function and plantar pressure measurement during 3D foot arch image acquisition in order to generate novel and more realistic clinical indices for clinical flat foot studies.

Acknowledgements

References

[1] P.R. Cavanagh, M.M. Rodgers, The arch index: a useful measure from footprints, Biomechanics 20 (1987) 547—551.

[2] W.M. Glasoe, H.J. Yack, C.L. Saltzman, Anatomy and biomechanics of the first ray, Phys. Ther. 79 (1999) 854—859.

[3] S.L. James, B.T. Bates, L.R. Osternig, Injuries to runners, Am. J. Sports Med. 6 (1987) 40—50.

[4] M. Giladi, C. Milgrom, M. Stein, H. Kashtan, J. Margulies, R. Chisin, R. Steinberg, Z. Aharonson, The low arch, a protective factor in stress fractures, Orthop. Rev. 14 (1985) 709—712.

[5] A. Simkin, I. Leichter, M. Giladi, M. Stein, C. Milgram, Combined effect of foot arch structure and an orthotic device on stress fractures, Foot Ankle 10 (1989) 25—29.

[6] A. Simkin, I. Leichter, Role of the calcaneal inclination in the energy storage capacity of the human foot—a biomechanical model, Med. Biol. Eng. Comput. 28 (1990) 149—152.

[7] M. Nordin, V.H. Frankel, Basic Biomechanics of the Musculoskeletal System, 2nd ed., Williams and Wilkins, 1989.

[8] C. Rene, Foot and Ankle Pain, Davis, 1992, pp. 83—86.

[9] C.L. Saltzman, D.A. Nawoczenski, K.D. Talbot, et al., Measurement of medial longitudinal arch, Arch. Phys. Med. Rehabil. 76 (1995) 45—49.

[10] U. Kanatli, H. Yetkin, E. Cila, Footprint and radiographic analysis of the feet, J. Pediatr. Orthop. 21 (2) (2001) 225—228.

[11] D.R. Wenger, D. Mauldin, G. Speck, et al., Corrective shoes and inserts as treatment for flexible flatfoot in infants and children, J. Bone Joint Surg. Am. 71 (1989) 800—810.

[12] M.W. Steel, K.A. Johnson, M.A. DeWitz, et al., Radiographic measurements of the normal adult foot, Foot Ankle 1 (1980) 152—158.

[13] R. Vanderwilde, L.T. Staheli, D.E. Chew, et al., Measurements on radiographs of the foot in normal infants and children, J. Bone Joint Surg. Am. 70 (1988) 407—415.

[14] G.W. Simons, A standardized method for the radiographic evaluation of clubfeet, Clin. Orthop. 70 (1978) 107—118.

[15] T.K. Cureton, J.S. Wickens, P.E. Haskell, The validity of footprints as a measure of vertical height of the arch and functional efficiency, Res. Quart. 6 (1935) 70—80.

[16] L.T. Staheli, D.E. Chew, M. Corbett, The longitudinal arch, Phys. Med. Rehabil. 69 (1978) 71—78.

[17] G.K. Rose, E.A. Welton, T. Marshall, The diagnosis of flat foot in the child, J. Bone Joint Surg. Br. 67 (1985) 71—78.

[18] M.R. Hawes, W. Nachbauer, D. Sovak, B.M. Nigg, Footprint parameters as a measure of arch height, Foot Ankle 13 (1992) 22—26.

[19] J.B. Volpon, Footprint analysis during the growth period, J. Pediatr. Orthop. 14 (1994) 83—85.

[20] U.B. Rao, B. Joseph, The influence of footwear on the prevalence of flat foot. A survey of 2300 children, J. Bone Joint Surg. Br. 74 (1992) 525—527.

[21] J.C. Cobey, E. Sella, Standardizing methods of measurement of foot shape by including the effects of subtalar rotation, Foot Ankle 2 (1981) 30—36.

[22] D.N. Ciwba, B.H. Jones, J.R. Robinson, Foot morphologic characteristics and risk of exercise-related injury, Arch. Fam. Med. 2 (1993) 773—777.

[23] D.N. Cowan, J.R. Robinson, B.H. Jones, D.W. Polly, B.H. Berrey, Consistency of visual assessments of arch height among clinicians, Foot Ankle 15 (1994) 213—217.

[24] R.I. Harris, T. Beath, Army foot survey: an investigation of foot ailments in Canadian soldiers, National Research Council of Canada, Ottawa, 1947.

[25] M. Sonka, V. Hlavac, R. Boyle, Image Processing, Analysis, and Machine Vision, International Thomson Publishing Company, 1998.

[26] R.C. Gonzalez, R.E. Woods, Digital Image Processing, Addison-Wesley, Reading, MA, 1993.

[27] A. Mojsilovic, B. Rogowitz, J. Gomes, T.S. Deisboeck, Analysis and 3D reconstruction of heterogeneity in malignant brain tumors: an interdisciplinary case study using a novel computational visualization approach, Anal. Quant. Cytol. Histol. 24 (2002) 125—133.

[28] S.A. Chu, T.I. Suvinen, J.G. Clement, P.C. Reade, The effect of interocclusal appliances on temporomandibular joints as assessed by 3D reconstruction of MRI scans, Aust. Dent. J. 46 (2001) 18—23.

[29] R.M. Cothren, R. Shekhar, E.M. Tuzcu, S.E. Nissen, J.F. Cornhill, D.G. Vince, Three-dimensional reconstruction of the coronary artery wall by image fusion of intravascular ultrasound and bi-plane angiography, Int. J. Card. Imaging 16 (2000) 69—85.

[30] A. Franke, H.P. Kuhl, P. Hanrath, Imaging techniques in cardiology: three-dimensional echocardiography, Z. Kardiol. 89 (2000) 150—159.

[31] F.J. Beekman, E.T. Slijpen, H.W. de Jong, M.A. Viergever, Estimation of the depth-dependent component of the point spread function of SPECT, Med. Phys. 26 (1999) 2311—2322.

[32] S.M. Yamany, A.A. Farag, D. Tasman, A.G. Farman, A 3D reconstruction system for the human jaw using a sequence of optical images, IEEE Trans. Med. Imaging 19 (2000) 538—547.

[33] B.L. Craine, E.R. Craine, C.J. O'Toole, Q. Ji, Digital imaging colposcopy: corrected area measurements using shape-from-shading, IEEE Trans. Med. Imaging 17 (1998) 1003—1010.

[34] S.R. Lehky, T.J. Sejnowski, Network model of shape-from-shading: neural function arises from both receptive and projective fields, Nature 2 (1988) 452—454.

[35] T.Y. Shiang, S.H. Lee, S.J. Lee, W.C. Chu, Evaluating different footprint parameters as a predictor of arch height, IEEE Eng. Med. Biol. Mag. 17 (1998) 62—66.